Research Article

Qingjie Lin, Yu Chen*, and Chao Liu

Mechanical properties of circular nano-silica concrete filled stainless steel tube stub columns after being exposed to freezing and thawing

https://doi.org/10.1515/ntrev-2019-0053
Received Dec 04, 2019; accepted Dec 20, 2019

Abstract: Experimental research on circular nano-silica concrete filled stainless steel tube (C-CFSST) stub columns after being exposed to freezing and thawing is carried out in this paper. All of forty specimens were tested in this paper, including nine C-CFSST specimens at normal temperature, 28 short columns of C-CFSST for freeze-thaw treatment and three circular hollow stainless steel stub columns. The failure mode, load-displacement curves, load-strain curves and load-bearing capacity were obtained and analyzed in this paper. The main parameters explored in the test include the number of freeze-thaw cycles (N=0, N=50, N=75, and N=100), wall thickness (T=1.0mm, T=1.2mm, T=1.5mm) andnano-silica concrete strength (f_c=20MPa, f_c=30MPa, f_c=40MPa). The result shows that C-CFSST short columns at normal temperature and subjected to freezing and thawing follow similar failure mode. The effect of freeze-thaw cycles (N) of 50 on bearing capacity of C-CFSST column was maximal, and then the influence of N on the bearing capacity of specimens was small when N reached to 75, finally the effect of N on bearing capacity of C-CFSST column was large when N reached to 100. The bearing capacity of C-CFSST columns increases with increasing wall thickness. In addition, the loss percentage of bearing capacity of specimens (f_c=40MPa) for freeze-thaw treatment is maximal, and the loss percentage of bearing capacity of specimens (f_c=30MPa) for freeze-thaw treatment is minimal. According to the test results, this paper proposed a formula to calculate the bearing capacity of C-CFSST short columns for freeze-thaw treatment.

Keywords: Circular nano-silica concrete filled stainless steel tube; Load bearing capacity; Freezing and thawing

Nomenclature

f_c Nano-silica concrete strength
C-CFSST Circular nano-silica concrete-filled stainless steel tube
E_s Elastic modulus of steel
D Outside diameter of circular stainless steel tube
H Height of the column
N Number of freezing and thawing cycles
N_u Ultimate strength of specimens
N_{eu} Experimental ultimate load-bearing capacity
N_{au} Ultimate strength of C-CFSST stub columns without being exposed to freezing and thawing
N_{cu} Calculated ultimate load-bearing capacity of C-CFSST stub columns after being exposed to freezing and thawing
Per Percentage of force decrease
f_y Yield strength of stainless steel
f_u Tensile strength of stainless steel
Δ_y Yield displacement of C-CFSST stub columns
Δ_u Ultimate displacement of C-CFSST stub columns
T Wall thickness of C-CFSST stub columns
Kr Reduction coefficient
α Parameter of nano-silica concrete strength
β Diameter-thickness ratio

1 Introduction

Nanotechnology has been considered as a main hub for the convergence and multidisciplinarity of research fields [1]. The implementation of fluorescent silica nanoparticles in the laboratory curriculum is introduced by Rashwan *et al.* [2]. State-of-the-art achievements on

***Corresponding Author: Yu Chen:** College of Civil Engineering, Fuzhou University, Fuzhou, China (350116); Email: yuchen@fzu.edu.cn; Tel.: +86 18030219629

Qingjie Lin: College of Civil Engineering, Fuzhou University, Fuzhou, China (350116)
Chao Liu: School of Urban Construction, Yangtze University, Jingzhou, China (434023)

typical low-dimensional nanostructured PDs and hybrid PDs are reviewed by Li, Zhenhui *et al.* [3]. Pawłowski *et al.* [4] proposed thermal silver plating method by means of nanosilver-based paint could be an alternative to electrochemical processes. John Chelliah *et al.* [5] highlighted the importance of the III–V semiconductor nanostructured channel in MOSFET [5]. Zhang Hailei [6] expanded the applications of halloysite nanotubes. Recently, nanoconcrete has also received more and more attention. This is also driving the use of nanotechnology in infrastructure. Many scholars mixed nanomaterials into concrete to obtain better performance of modified concrete [7–9]. And the nano-silica concrete used in this paper is one of them. Adding nano silica to concrete can make it more compact, increase the strength in the early stage, enhance the toughness, and significantly improve the durability of concrete.

Nowadays, concrete filled stainless steel tube columns are widely used in civil engineering, for example, the offshore engineering and bridge engineering owing to its high strength. Many researchers performed study on the performance of concrete filled stainless steel tube columns. Hassanein *et al.* [10] conducted parametric study on the behavior of concrete-filled double skin tubular slender columns. Vipulkumar *et al.* [11] carried out a test on circular concrete–filled stainless steel tubular slender beam-columns, and the result showed that the axial strength of slender columns is found to increase by using stainless steel tubes. Han *et al.* [12] conducted a study on the performance of stainless steel-concrete-carbon steel double-skin tubular columns. Brian *et al.* [13] investigated the behavior of short and slender concrete-filled stainless steel tubular columns, which showed that the composite members have potential to be extensively used as structure members. Zhao *et al.* [14] conducted a study on the performance of stainless steel circular hollow sections. Yuan *et al.* [15] investigated the residual stress distributions of welded stainless steel. Jandera *et al.* [16] investigated the influence of residual stress on behavior of stainless steel.

The freezing and thawing is a worldwide problem that affects the load-bearing capacity and ductility of a series of structures. For example, in recent years, there have been many low temperature damage accidents of CFST columns in northern China. This result is due to the fact that the mechanical behavior of CFST columns subjected to cycle of freeze-thaw became bad. So it is of great importance to conduct a study on the performance of C-CFSST columns subjected to cycle of freeze-thaw. In addition, freezing and thawing is an important factor to reduce the service life of buildings in offshore Engineering. In every seaport of North of China, the concrete in structures So it is of great importance to conduct a study on the performance of C-CFSST columns subjected to cycle of freeze-thaw was damaged.

In recent years, many tests have been conducted to investigate behavior of different materials subjected to freeze-thaw cycles. The research on CFST stub columns subjected to cycle of freeze-thaw was carried out by Yang *et al.* [17], which indicates that the specimens without being exposed to freeze-thaw cycles performed a better property than those specimens subjected to cycle of freeze-thaw. Li *et al.* [18] conducted a test on marine concrete subjected to freezing and thawing, which indicates that the freeze-thaw cycles accelerated chloride ion corrosion; it could be found that chloride ions could reduce the freezing resistance of concrete. Vesa *et al.* [19] conducted a test to investigate the stress and state of concrete, which verified the assumption of the critical degree of saturation of the pore system, that freezing and thawing can accumulate residual expansion. Tian *et al.* [20] performed the flexural load on self-compacting concrete under salt freezing and thawing cycles. The result showed that the bigger stress levels will cause earlier brittle failure. And this paper proposed a prediction model of degree of damage of self-compacting concrete. Shang *et al.* [21] conducted a study on steel bar in recycled coarse aggregate concrete under fast freezing and thawing in fresh water or sea water, including sixty-three specimens. Rami H *et al.* [22] conducted many tests to investigate the effect of freeze-thaw cycles and alkali-silica reaction on concrete-steel bond, which found that the alkali-silica reaction caused a great decrease in critical bond stress of specimens. Shang *et al.* [23] performed biaxial compression on plain concrete subjected to freeze-thaw cycles to investigate the deformation and strength of concrete, and proposed a useful formula to predict biaxial compressive strength in principal stress space. Marcelo *et al.* [24] presented an experimental investigation on Portland cement concrete; the experimental result showed that the freezing and thawing can affect the durability of concrete.

There are many researches about mechanical properties of nano-silica concrete [25–27] and a lot of researches about concrete filled steel tube stub columns after being exposed to freezing and thawing [17, 28], but there are very few studies on the performance of nano-silica concrete filled stainless steel tube (CFSST) columns subjected to freeze-thaw cycles. So it is important to conduct a test on the behavior of CFSST columns subjected to freeze-thaw cycles. This paper mainly investigated the ultimate strength of C-CFSST stub columns subjected to freeze-thaw cycles under axial load. According to the experimental results, a formal was presented to calculate the ultimate

(a) Beaker **(b)** Hydrophilic-380 type **(c)** Dissolve

Figure 1: Nano silica ratio production

load-bearing capacity of CFSST stub columns subjected to freeze-thaw cycles.

2 Experimental program

2.1 Specimen preparation

All forty specimens were tested in this paper, including nine circular nano-silica concrete filled stainless steel tubes at ambient temperature, three hollow stainless short columns at ambient temperature and twenty-eight circular nano-silica concrete filled stainless steel tube exposed to freezing and thawing. The nano-silica adopts the hydrophilic gas phase nano-silica (Hydrophilic-380 type), with a specific surface area of 390mm^2/g and a particle size of 6-45nm. In engineering practice, adding 1% nano-silica can better improve the mechanical properties of circular nano-silica concrete filled stainless steel tube (C-CFSST) stub columns for freeze-thaw treatment, so the parameter of nano-silica in this test is 1%. The preparation process of nano-silica ratio is shown in Figure 1. The details of specimens are presented in Table 1. The nominal size of specimens (D×H) for the C-CFSST is 89×300mm, where D is the outside diameter of specimens; H is the height of specimens. The main parameters in the test include:

- Number of freeze-thaw cycles: 0, 50, 75 and 100.
- Wall thickness of stainless steel tube: 1.0mm, 1.2mm and 1.5mm.
- Strength grade of nano-silica concrete: 20MPa, 30MPa and 40MPa.

2.2 Specimen labeling

All specimens were labeled according to the strength grade of nano-silica concrete, wall thickness of stainless steel, number of freezing and thawing cycles. For instance, the C20-T1.0-N0 is defined as follows:

- The first part of the label“C20” denotes that the strength grade of nano-silica concrete is 20MPa.
- The second part of the label “T1.0” denotes that the wall thickness of stainless steel is 1.0mm.
- The last part of the label “N0” denotes that the number of freeze-thaw cycles is 0.

2.3 Material properties

All stainless steel tubes are made of 201 austenitic stainless steel. Three long stainless steel tubes (T=1.0mm, 1.2mm and 1.5mm) are used for manufacturing the stub columns. The tensile coupons test was conducted to determine the tensile strength of stainless steel (f_u), yield strength of stainless steel (f_y), according to the test procedures of the Chinese Standard of Metallic Materials (GB/T 228-2002) [29]. The tensile coupons test was conducted at normal temperature and all tensile coupons were extracted from the left long stainless steel pipes. The performance of stainless steel is shown in Table 2.

The bottom of the stainless steel tube was covered with a layer of water proof cloth, and then, the nano-silica concrete was pumped from the top into the stainless steel tube. The nano-silica concrete was vibrated and was leveled before finishing in order to ensure that it was well compacted. In second day, the top of specimens were cased over with cement mortar to ensure that the bottom of the specimens is flat. The detailed nano-silica concrete mixes were listed in Table 3. At the same time, three nano-silica

Table 1: Details of specimens

Specimen labels	H(mm)	T(mm)	N	D(mm)	f_C(MPa)
C0-T1.0-N0	300	1.0	0	89	0
C0-T1.2-N0	300	1.2	0	89	0
C0-T1.5-N0	300	1.5	0	89	0
C20-T1.0-N0	300	1.0	0	89	20
C20-T1.0-N50	300	1.0	50	89	20
C20-T1.0-N75	300	1.0	75	89	20
C20-T1.0-N100	300	1.2	100	89	20
C20-T1.2-N0	300	1.2	0	89	20
C20-T1.2-N50	300	1.2	50	89	20
C20-T1.2-N75	300	1.5	75	89	20
C20-T1.2-N100	300	1.5	100	89	20
C20-T1.5-N0	300	1.5	0	89	20
C20-T1.5-N50	300	1.0	50	89	20
C20-T1.5-N75	300	1.0	75	89	20
C20-T1.5-N100	300	1.0	100	89	20
C30-T1.0-N0	300	1.2	0	89	30
C30-T10-N50	300	1.2	50	89	30
C30-T1.0-N75	300	1.2	75	89	30
C30-T1.0-N100	300	1.5	100	89	30
C30-T1.2-N0	300	1.5	0	89	30
C30-T1.2-N50	300	1.5	50	89	30
C30-T1.2-N75	300	1.0	75	89	30
C30-T1.2-N100	300	1.0	100	89	30
C30-T1.5-N0	300	1.0	0	89	30
C30-T1.5-N50	300	1.2	50	89	30
C30-T1.5-N75	300	1.2	75	89	30
C30-T1.5-N100	300	1.2	100	89	30
C40-T1.0-N0	300	1.5	0	89	40
C40-T1.0-N50	300	1.5	50	89	40
C40-T1.0-N75	300	1.5	75	89	40
C40-T1.0-N100	300	1.0	100	89	40
C40-T1.2-N0	300	1.0	0	89	40
C40-T1.2-N50	300	1.0	50	89	40
C40-T1.2-N75	300	1.2	75	89	40
C40-T1.2-N100	300	1.2	100	89	40
C40-T1.5-N0	300	1.2	0	89	40
C40-T1.5-N50	300	1.5	50	89	40
C40-T1.5-N75	300	1.5	75	89	40
C40-T1.5-N100	300	1.5	100	89	40
C40-T1.0-N75	300	1.0	75	89	40

concrete cubes with dimension of 150mm×150mm×150mm were made to test the nano-silica concrete strength. The nano-silica concrete cubes were conducted to load test after finishing twenty-eight-day curing of the concrete. The test results were given in Table 4.

2.4 Freeze-thaw test

The fast freezing and thawing test method according to the China standard GB/T 50082–2009 (2009) [30] was applied in freezing and thawing test because the nations have not issued freezing and thawing test standard. All twenty-

Table 2: Properties of stainless steel tube

Specimen(mm)	f_y(Mpa)	f_u(Mpa)	f_y/f_u
T=1.0	350	412	0.85
T=1.2	423	508	0.83
T=1.5	531	649	0.82

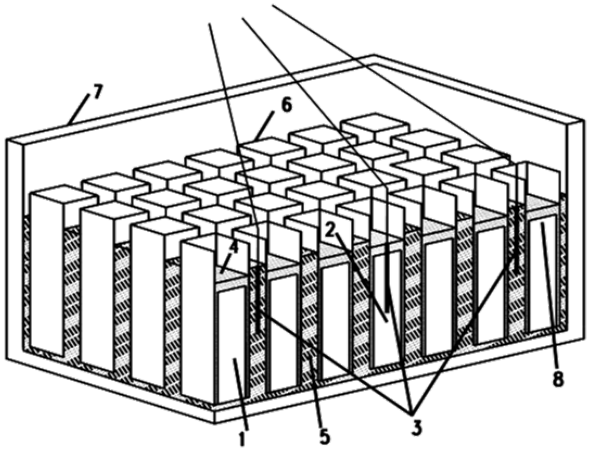

Figure 2: Freezing and thawing device:1-Specimen; 2-Specimen for core temperature measurement; 3-Thermocouples; 4-Water; 5-Antifreeze fluid; 6-Rubber box; 7-Container

eight specimens were put into fast freeze-thaw device, in which one specimen was used to test the core temperature of specimens. The schematic diagram of fast freeze-thaw testing device is shown in Figure 2. The core temperature of the specimen is between –20 and 15°C; the time of a cycle is four to six hours and ensure that all specimens are exposed to the whole process of freezing-thawing cycle. The freeze-thaw test lasted twenty-one days. In the test, there are some technical indexes and parameters as follows:

- The minimum and maximum temperatures of the specimen center were –17.6°C±3°C and 8°C±6°C.
- The time of temperature decreased from 8°C to 17.6°C accounted for a half of freezing time of freezing-thawing cycles, and the time of temperature rising from –17.6°C to 8°C accounted for a half of heating time of freezing-thawing cycles.
- The temperature variation between the center and the surface of specimens does not exceed 28°C.
- The conversion between the freezing and thawing is not more than twenty minutes.

The specimens were placed into device after curing period, and all specimens were immersed into water. When the number of freezing-thawing cycles was up to fifty, seventy-five, and one hundred, the specimens were removed from the machine. And then water on the surface of specimens was wiped up. The freeze-thaw test was stopped when the number of freezing-thawing cycles was 100. It was found that:

(a) Before freezing and thawing

(b) After freezing and thawing

Figure 3: Cement mortar before and after being exposed to freezing and thawing

- Specimens had no obvious deformation and there was not rusty phenomenon on the stainless steel tube.
- The cement mortar at bottom of the specimens fell off.

The cement mortar at bottom of specimens for freeze-thaw cycle treatment has fallen off, as seen from Figure 3. In addition, the freezing and thawing cycles measured within 24 hours are shown in Figure 4.

Table 3: Nano-silica concrete mix proportions

Strength grade of nano-silica concrete	Water (kg/m^3)	Cement (kg/m^3)	Sand (kg/m^3)	Gravel (kg/m^3)	Nano silica content (%)
C20	185	350	650	1180	1
C30	183	450	600	1192	1
C40	178	520	525	1220	1

Table 4: Result of nano-silica concrete stress test

Strength grade of nano-silica concrete cube	f_{u1}(MPa)	f_{u2}(MPa)	f_{u3}(MPa)	Mean value(MPa)
C20	22.3	23.8	24.4	23.5
C30	35.2	35.5	36.1	35.6
C40	41.4	42.1	43.4	42.3

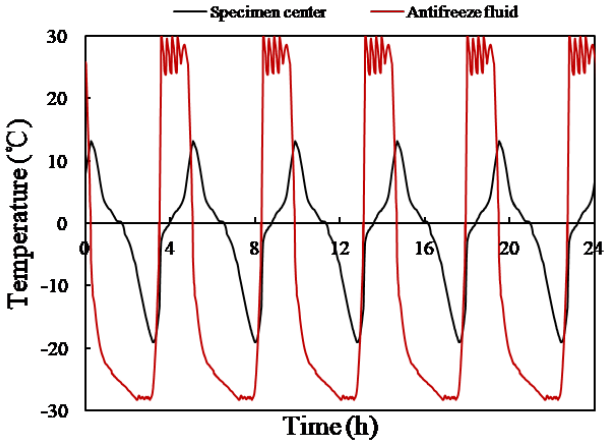

Figure 4: The temperature of freeze-thaw cycles within 24 hours

2.5 Axial compression on specimens

After finishing the freezing and thawing, all specimens were tested by Electro-hydraulic servo universal testing machine with the ultimate load bearing capacity of 1000kN, as shown in Figure 5. First, the specimens was placed on the support and made the specimens parallel to the plate, then connected to the DH3816 to ensure the balance of the strain gages. Finally, the specimens were under axially loaded and the strain data were recorded regularly during the test.

In order to better study the strain of the specimens, local strain distribution was obtained by strain gauge method. Strain gages were used for nine test specimens (C20-T1.5-N75, C30-T1.5-N0, C30-T1.5-N50, C30-T1.5-N75, C30-T1.5-N100, C40-T1.0-N50, C40-T1.2-N50, C40-T1.5-N50, and C40-T1.5-N75.). The strain gages were placed on the two locations with interval of 90° at middle of the outer

Figure 5: Device of loading test

surface of the specimens. Total of four strain gages were used for each specimens, as shown in Figure 6.

All specimen strain gages are connected to the DH-3816. In order to ensure the balance of the strain gage, the strain value collected before loading should be between −10 and +10. The specimens were loaded at a rate of 0.5kN/s until failed. The load interval is 1/10 of the limit bearing capacity of specimens when the material is in the elastic range, and the load interval is 1/20 of the limit bearing capacity when the load is up to 80% of load-bearing capacity. Each interval was maintained for 1~2 minutes. All specimens after load test are shown in Figure 7.

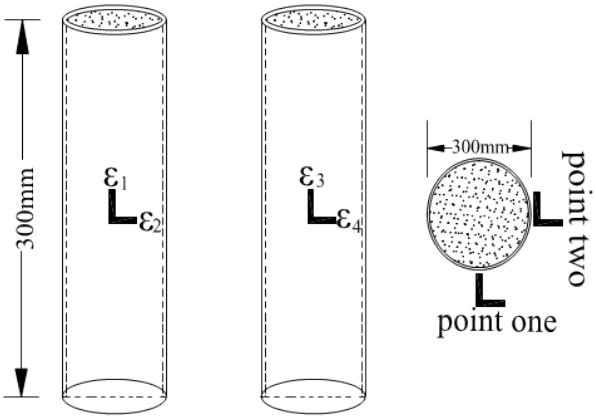

Figure 6: Arrangement of strain gages

Figure 7: All specimens after axial compression

3 Test result

3.1 Failure modes

When the load reached to eighty percent of limit bearing capacity, some small deformation appeared at bottom of the specimens. Some obvious deformation appeared at surface of the specimens as the load increases. When the load reached to ninety percent of limit bearing capacity, there was obvious buckling around the center or the bottom of the specimens. When the load was up to ultimate bearing capacity of the specimens, there was some axial displacement occurring in specimens.

The thermal expansion coefficient of stainless steel is similar to that of concrete, so under the influence of freeze-thaw, the deformation of stainless steel tube and concrete is close. The shrinkage deformation of the stainless steel tube is close to that of the inner core concrete, so the transverse binding force exerted by the stainless steel tube on the inner core concrete does not change much and all specimens with different number of freezing and thawing cycles have similar failure mode.

However, the positions of local buckling happened to the specimens are different, as illustrated in Figure 8. As shown from Figure 8(a), the bottom of specimens is complete, and the upper of specimens presents obvious buckling in surface of specimens, which was named mode one. Mode two was shown in Figure 8(b), there is obvious buckling around whole specimens, and specimens have obvious axial deformation. The number of specimens of mode one and mode two is total of fourteen and twenty-three respectively. In addition, the nano-silica concrete at bottom and the top of the specimens after load is complete, which was illustrated in Figure 8(c).

Figure 9 shows the failure mode of circular hollow stainless steel tube. It shows that there is a certain buckling at the top of the stainless steel hollow short columns, and the bottom and middle part of short columns are complete.

3.2 Load-displacement curves

In order to evaluate the influence of three parameters on the mechanical behavior of specimens, the axial deformation (Δ) versus load (P) curves of the columns was shown in Figure 10. All curves have two stages: elastic stage and elastic-plastic stage.

As seen from Figure 10, the wall thickness and nano-silica concrete strength are the key influence factor of ultimate loads of specimens for freeze-thaw treatment. As seen from Figure 10(a), 10(b), 10(c), 10(d), and 10(e), the influence of the number of freezing-thawing cycles on the limit bearing capacity of the specimen was discrete. As seen from Figure 10(a), 10(b), 10(c) and 10(d), the freezing and thawing reduced the initial stiffness of specimens, and the initial stiffness of the specimen decreases as the freezing-thawing cycle's number increases. As seen from Figure 10(f), 10(g), 10(h), 10(i), the curves of specimens for freeze-thaw treatment were basically similar. The limit bearing capacity of specimens with T=1.5mm is larger than that of another specimens with T=1.2mm and T=1.0mm, which shows that the limit bearing capacity of specimens improve as wall thickness increases. As seen from Figure 10(j), 10(k), and 10(l), it shows that the limit bearing capacity of C-CFSST specimens increases with the increase of nano-silica concrete strength. In addition, it was found that, as the thickness of the wall increases, the negative effect of freezing and thawing on initial stiffness of C-CFSST stub columns became small from the comparison among Figure 10(a), 10(b), and 10(c). With the improve-

(a) Failure mode one

(b) Failure mode two

(c) The bottom of the specimens after loading test

(d) The bottom failure phenomenon

Figure 8: Typical failure modes and the bottom failure phenomenon

ment of nano-silica concrete strength, the negative effect of freezing and thawing on initial stiffness of C-CFSST stub columns became small from the comparison among Figure 10(a), 10(d), and 10(e).

3.3 Load-strain curves

Figure 11 shows the load-strain curves of C-CFSST stub columns. The solid line refers to the value of strain of point one of specimens and the dash line refers to the value of strain at point two of specimens. As seen from Figure 11(a), for the C30-T1.5-N75 and C30-T1.5-N0, the rate of increase in strain values of the specimen (N=75) is larger than that of strain values of the specimen (N=0). The rate of increase in value of strain of specimens (N=75) is larger than the rate of increase in value of strain of specimens (N=100). It shows that the rate of increase in value of strain of specimens for freeze-thaw treatment is respectively greater than the rate of increase in value of strain of specimens at ambient temperature. The value of strain of specimens (f_c=30MPa) subjected to cycle freeze-thaw under same load is respectively smaller than value of strain of specimens at normal temperature, which indicates that the behavior of deformation resistance of speci-

(a) Axonometric view **(b)** Front view

Figure 9: Failure mode of hollow stainless steel tube

mens (f_c=30MPa, T=1.5mm) was improved by freezing and thawing.

Figure 11(b) shows the comparison of load-strain curves of different nano-silica concrete strength. As seen from this figures, the rate of increase in numerical axial and transverse strain values of specimens (f_c=20MPa) at point two is smaller than the rate of increase in numerical value of axial and transverse strain values of specimens (f_c=30MPa and f_c=40MPa), which indicates that the strain of axial and lateral of specimens (f_c=20MPa) at point two is worse than strain of axial and lateral of specimens (f_c=30MPa and f_c=40MPa). The rate of increase in numerical axial and transverse strain values for specimens (f_c=30MPa) is basically equal to specimens with f_c=40MPa, which indicates that the number of freeze-thaw cycles has greater effect on core concrete of specimens (f_c=40MPa) than core concrete of specimens (f_c=30MPa).

It could be seen that the comparison of load-strain curves of different thickness from Figure 11(c). It could be found that the limit bearing capacity of specimens (T=1.0mm) is basically equal to that of specimens (T=1.2mm), and the specimens (T=1.5mm) have the largest limit bearing capacity, which indicates that the specimens (T=1.5mm) have the largest load-bearing capacity. When load reached to ultimate bearing capacity of specimens, the maximum strain of specimens (T=1.5mm) is greater than the maximum strain of specimens (T=1.2mm and T=1.0mm), and the maximum strain of specimens (T=1.2mm) is greater than the maximum strain of specimens (T=1.0mm). As seen from Figure 11(c), the greater the wall thickness is, the better ductility the specimens have. As a result, the behavior of specimens was improved by wall.

Generally speaking, the change rule of lateral strain is similar to that of axial strain.

4 Analysis of test result

All test results of all specimens tested in this paper are shown in Table 5. The experimental ultimate strength (N_u), percentage of force decrease (*Per*), yield strength (N_y), yield displacement (Δ_y), ultimate displacement (Δ_u) and ductility coefficient (Δ_u/Δ_y) are presented in Table 5.

4.1 Effect of number of freezing and thawing cycles

As seen from Figure 10, Figure 12 and Table 5, the effect of freezing and thawing cycles (N) on load-bearing capacity of specimens is discrete. As seen from Figure 10(a) and 10(b), the initial stiffness of specimens (N=100) for freeze-thaw cycles treatment is smaller than that of specimens (N=75, N=50 and N=0), and the initial stiffness of specimens at normal temperature is larger than the initial stiffness of specimens subjected to freeze-thaw cycle, which indicates that the number of freezing-thawing cycles reduced the initial stiffness of C-CFSST stub columns. In addition, as shown in Figure 10(a), 10(b) and 10(c), the

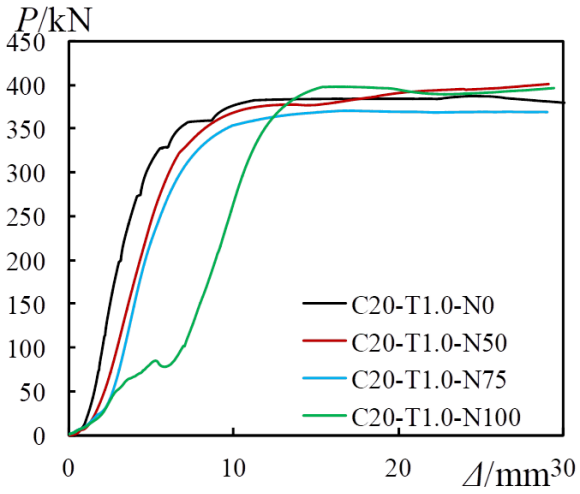

(a) f_c=20MPa, T=1.0mm

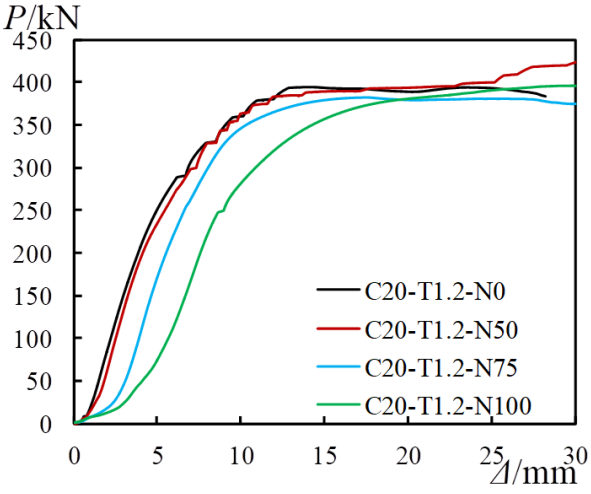

(b) f_c=20MPa, T=1.2mm

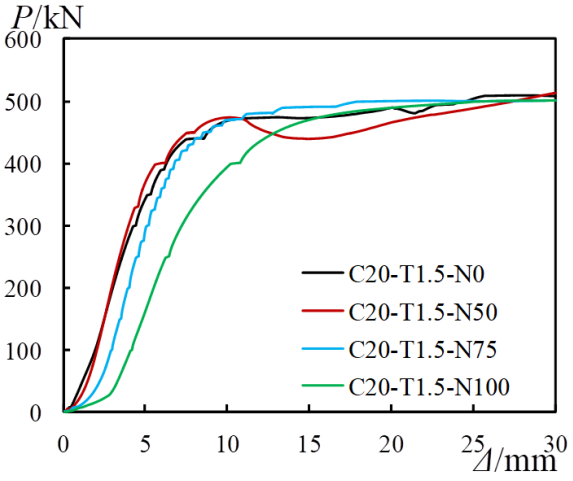

(c) f_c=20MPa, T=1.5mm

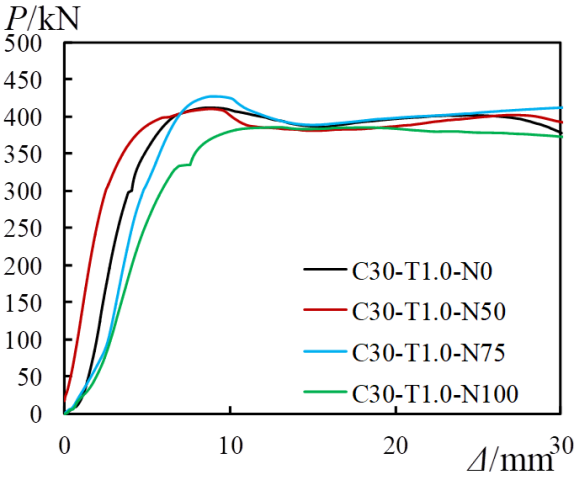

(d) f_c=30MPa, T=1.0mm

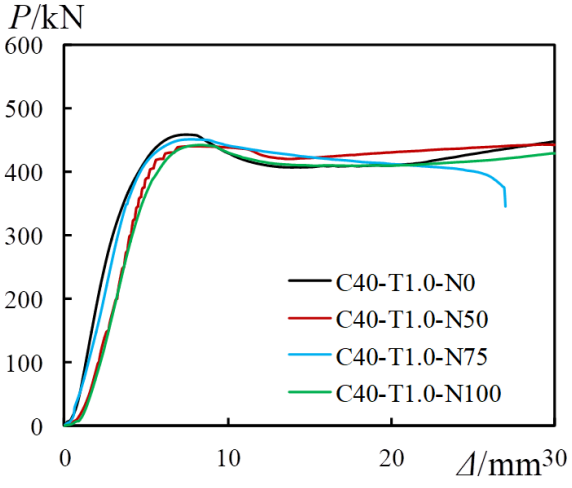

(e) f_c=40MPa, T=1.0mm

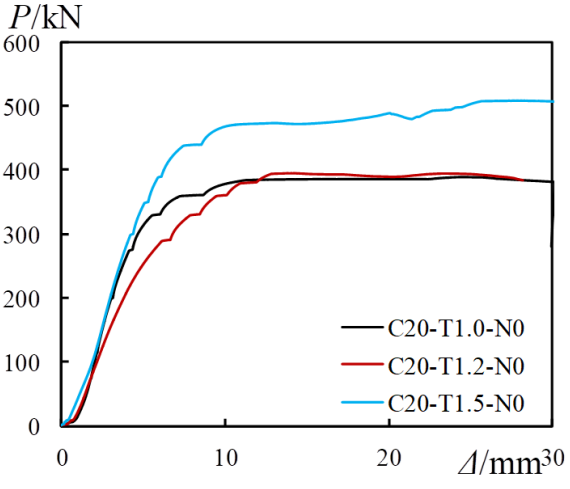

(f) f_c=20Mpa, N=0

Figure 10: Load-displacement curves

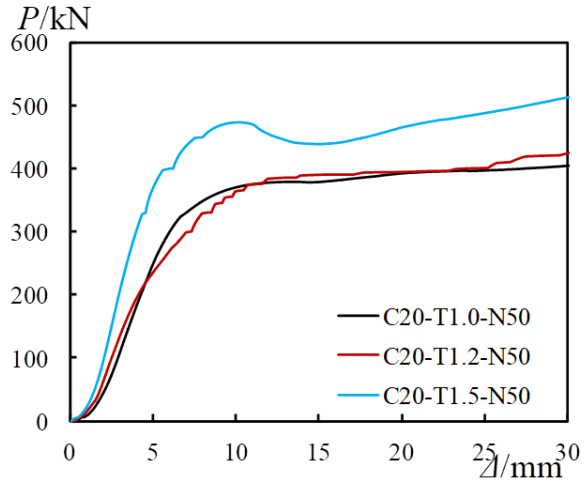

(g) f_c=20MPa, N=50

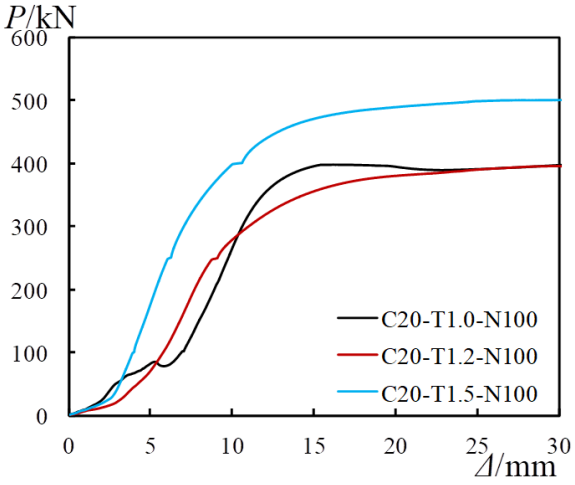

(h) f_c=20MPa, N=100

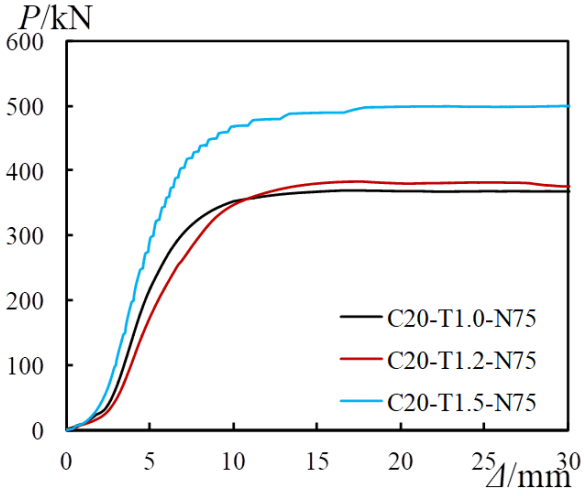

(i) f_c=20MPa, N=75

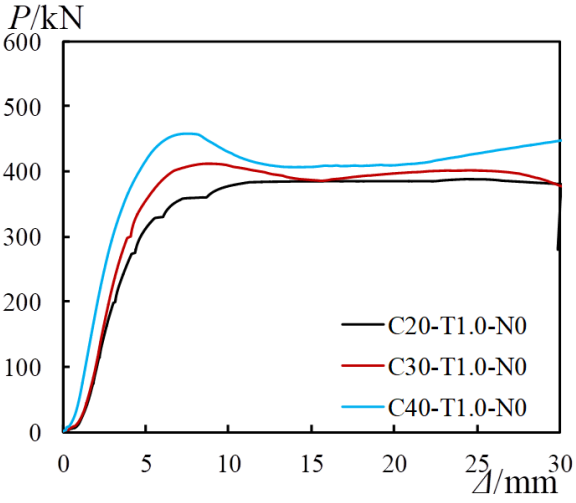

(j) T=1.0mm, N=0

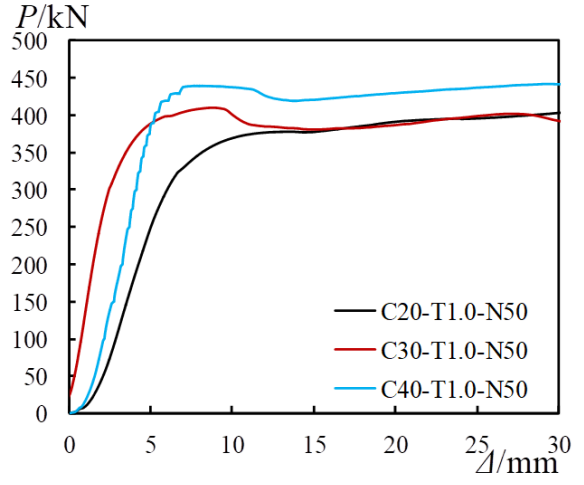

(k) T=1.0mm, N=50

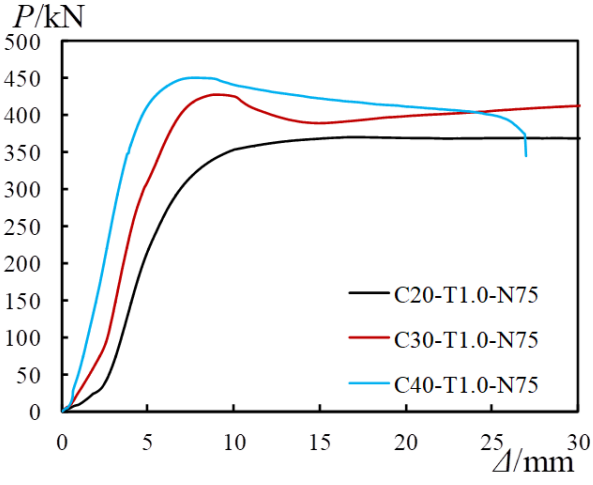

(l) T=1.0mm, N=75

Figure 10: ...continued

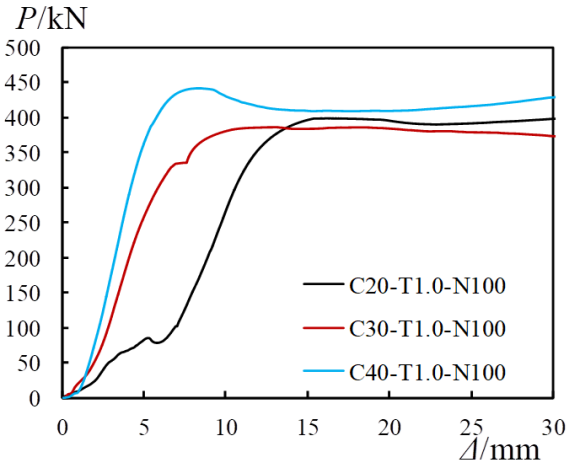

(m) T=1.0mm, N=100

Figure 10: ...continued

effect of freezing and thawing cycle on initial stiffness of C-CFSST stub columns became smaller with the improvement of wall thickness (T). The percentage loss of ultimate bearing capacity increases from −12.63% to 10.64% when the N ranges from 0 to 100, as listed in Table 5.

As seen from Figure 10(b), the specimens (N=100), the elastic stage of specimens (N=100) is shorter than elastic stage of specimens with another N, which indicates that the N could reduce the deformation resistance of specimens with small nano-silica concrete strength and small wall thickness.

As seen from Figure 10(a), 10(d) and 10(e), similar to specimens without being exposed to cycle of freeze-thaw, the C-CFSST stub columns subjected to cycle of freeze-thaw usually have steady load versus displacement curves. It could be found that the influence of N on initial stiffness of specimens became smaller with the improvement of nano-silica concrete strength. In addition, the influence of N of 100 on initial stiffness of specimens (T=1.0mm and f_c=20MPa, T=1.0mm and f_c=30MPa) is the greatest, but the influence of N of 50 and 100 on initial stiffness of specimens (T=1.0mm and f_c=40MPa) is the greatest, which means that the damage of the material does not increase as the freeze-thaw cycles increase.

As seen from Table 5, the limit bearing capacity of some specimens subjected to cycle of freeze-thaw was improved, especially for specimens with f_c=30MPa and T=1.5mm, the improvement of ultimate bearing capacity is great. The maximum percentage of increase in load-bearing capacity reached to 12.63%. It can be explained that the freezing and thawing has particular effect on the core concrete due to the particular mix proportion of C30 and the fact that the constraining effect to core concrete

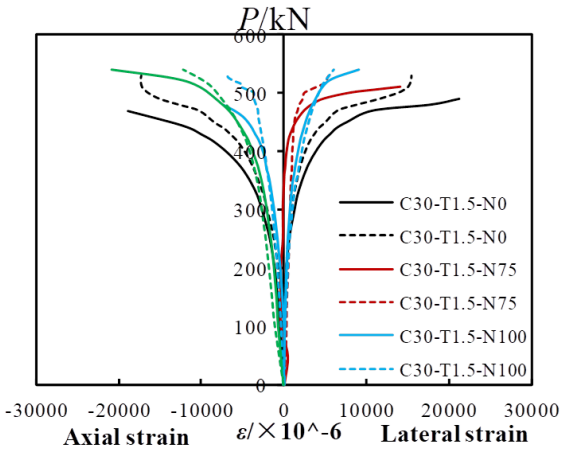

(a) Load-strain curves of different N

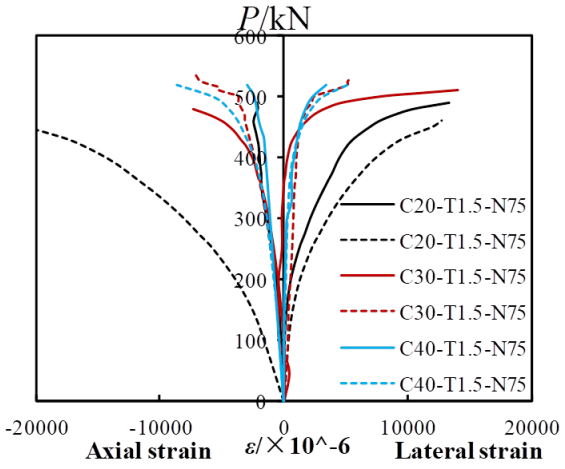

(b) Load-strain curves of different f_c

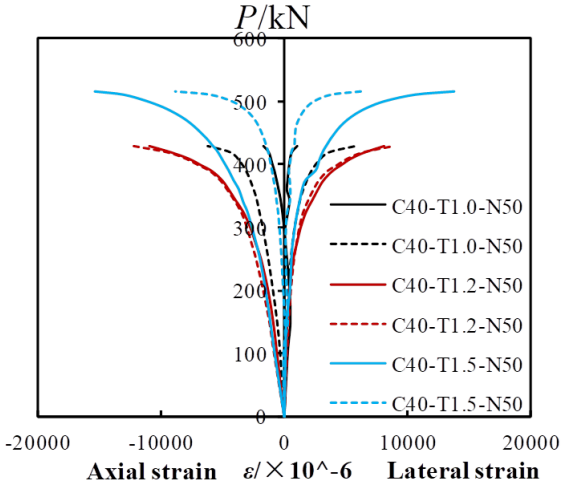

(c) Load strain curves of different T

Figure 11: Load-strain curves

Table 5: Experimental result for all specimens

Specimen labels	N_u (kN)	*Per*	N_y(kN)	Δ_y(mm)	Δ_u(mm)	Δ_u/Δ_y
C20-T1.0-N0	385.00	0%	288.75	4.50	20	4.44
C30-T1.0-N0	412.10	0%	309.08	4.13	20	4.84
C40-T1.0-N0	478.25	0%	358.69	3.80	20	5.26
C20-T1.2-N0	394.20	0%	295.65	6.75	20	2.96
C30-T1.2-N0	481.10	0%	360.83	4.90	20	4.08
C40-T1.2-N0	492.10	0%	369.08	3.26	20	6.13
C20-T1.5-N0	487.35	0%	365.51	5.48	20	3.65
C30-T1.5-N0	498.55	0%	373.91	4.87	20	4.11
C40-T1.5-N0	575.45	0%	431.59	4.83	20	4.14
C20-T1.0-N50	389.15	−1.08%	291.86	5.84	20	3.42
C30-T1.0-N50	409.85	0.55%	307.39	2.65	20	7.54
C40-T1.0-N50	439.90	8.02%	329.93	4.37	20	4.58
C20-T1.2-N50	393.85	0.09%	295.39	6.91	20	2.89
C30-T1.2-N50	440.70	8.40%	330.53	3.40	20	5.88
C40-T1.2-N50	439.75	10.64%	329.81	4.55	20	4.40
C20-T1.5-N50	473.15	2.91%	354.86	4.77	20	4.19
C30-T1.5-N50	524.60	−5.23%	393.45	6.80	20	2.94
C40-T1.5-N50	519.40	9.74%	389.55	6.13	20	3.26
C20-T1.0-N75	369.80	3.95%	277.35	6.22	20	3.22
C30-T1.0-N75	426.35	−3.46%	319.76	5.192	20	3.85
C40-T1.0-N75	449.95	5.92%	337.46	3.70	20	5.41
C20-T1.2-N75	382.25	3.03%	286.69	7.64	20	2.62
C30-T1.2-N75	433.35	9.93%	325.01	6.31	20	3.17
C40-T1.2-N75	500.40	−1.69%	375.30	4.38	20	4.57
C20-T1.5-N75	499.15	−2.42%	374.36	6.34	20	3.15
C30-T1.5-N75	539.65	−8.24%	404.74	4.87	20	4.11
C40-T1.5-N75	542.85	5.67%	407.14	4.36	20	4.59
C20-T1.0-N100	398.50	−3.51%	298.88	10.57	20	1.89
C30-T1.0-N100	385.65	6.42%	289.24	5.62	20	3.56
C40-T1.0-N100	441.10	7.77%	330.83	4.55	20	4.40
C20-T1.2-N100	379.15	3.82%	284.36	10.09	20	1.98
C30-T1.2-N100	445.40	7.42%	334.05	4.43	20	4.51
C40-T1.2-N100	466.15	5.27%	349.61	4.32	20	4.63
C20-T1.5-N100	488.65	−0.27%	366.49	8.98	20	2.23
C30-T1.5-N100	561.50	−12.63%	421.13	5.44	20	3.68
C40-T1.5-N100	541.70	5.86%	406.28	4.57	20	4.38

becomes better with the increase of wall thickness. In addition, on average, the influence of the N of 50 on bearing capacity is greatest, as seen from Table 5.

Figure 12 shows the influence of N on experimental bearing capacity of C-CFSST specimens with same nano-silica concrete strength. As seen from Figure 12(b), the experimental limit bearing capacity of specimens (f_c=30MPa and T=1.5mm) increases as the N increase. The limit bearing capacity of specimens (T=1.0mm and f_c=20MPa, T=1.2mm and f_c= 20MPa) decreased when the N reached to 75. The limit bearing capacity of specimens (f_c=40MPa) decreased when the N reached to 50. In addition, it could be seen that the specimens (T=1.5mm) always have the largest ultimate bearing capacity, the limit bearing capacity of specimens (T=1.2mm) is larger than bearing capacity of specimens (T=1.0mm), which indicates that the limit bearing capacity of specimens increases as the wall thickness improves. On average, the specimens (T=1.0mm and T=1.2mm) subjected to cycle of freeze-thaw had lower the limit bearing capacity over the specimens without being

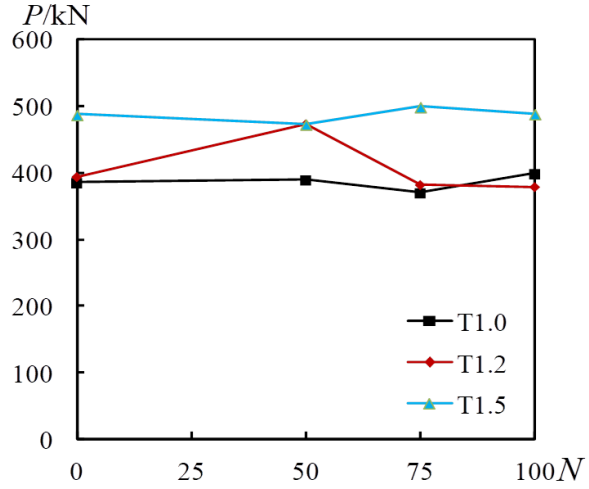

(a) f_c=20MPa

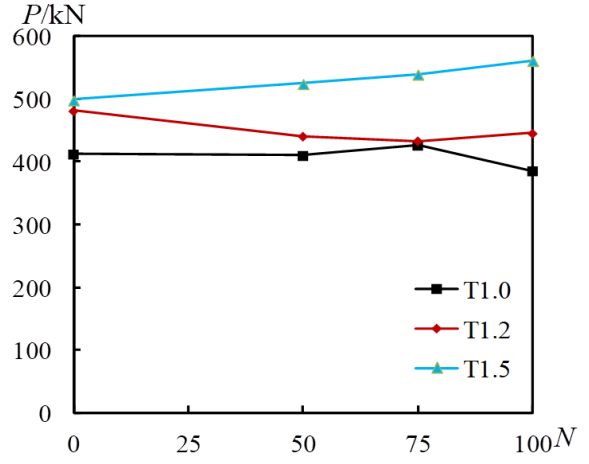

(b) f_c=30MPa

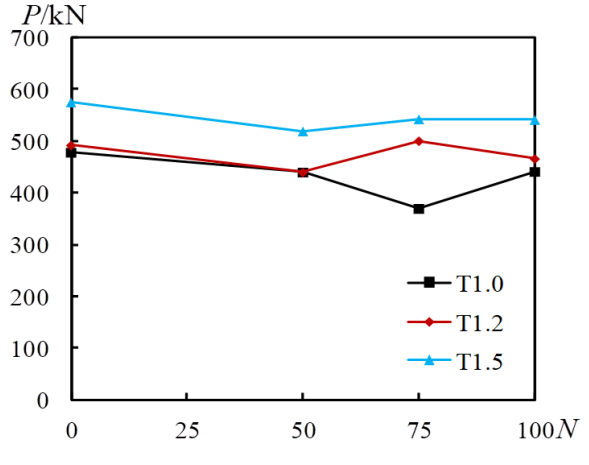

(c) f_c=40MPa

Figure 12: *P-N* curves

exposed to cycle of freeze-thaw by 2.23% to 5.21%. It can be explained that under the influence of freeze-thaw the remaining water of unhydrated cement results in the generation and development of micro-cracks in the concrete, which reduces the compressive strength of concrete.

4.2 Effect of nano-silica concrete strength

Figure 10(j), 10(k), 10(l) and 10(m) shows load-displacement curves of different nano-silica concrete strength in the same wall thickness (T) and number of freezing-thawing cycles (N). The specimens with f_c=40MPa have the greatest ultimate load-bearing capacity, which shows that the specimens with high nano-silica concrete strength have larger ultimate bearing capacity than the specimens with low nano-silica concrete strength. It can be explained that the specimens with higher concrete strength grade have a smaller water-cement ratio and therefore have less residual freezable water content. Thus freezing-thawing cycle has less influence on the strength of specimens with high nano-silica concrete strength. As seen from Figure 11(b), the specimens with f_c=20MPa have lowest rate of increase in numerical value of lateral and axial strains at point two, and it can be seen from Table 5 that on average, the C-CFSST stub columns with f_c=20MPa have minimum ultimate bearing capacity in the same T and N, which means that the specimens with f_c=20MPa have the worst mechanical behavior in the same T and N.

Figure 13(a), 13(b), and 13(c) show the effect of nano-silica concrete strength (f_c) on limit bearing capacity of specimens with same wall thickness. As seen from Figure 13(a), except the specimen with N=75, the curves have an uptrend with the increase of f_c. As seen from Figure 13(b) that except the specimen with N=50, the curves have an uptrend with the increase of f_c. On average, the limit bearing capacity increases as the strength grade of nano-silica concrete increases. In addition, as seen from Figure 13(c), the limit bearing capacity of specimens with f_c=30MPa and T=1.5mm subjected to cycle of freeze-thaw is greater than the limit bearing capacity of specimens with f_c=30MPa and T=1.5mm without being subjected to cycle of freeze-thaw, which could be found that the strength of internal nano-silica concrete of specimens with f_c=30MPa and T=1.5mm subjected to freeze-thaw cycles was improved. The freezing and thawing has particular effect on internal nano-silica concrete of C-CFFST stub columns with f_c=30MPa and T=1.5mm due to the particular mix proportion and great constraining to core concrete provided by wall.

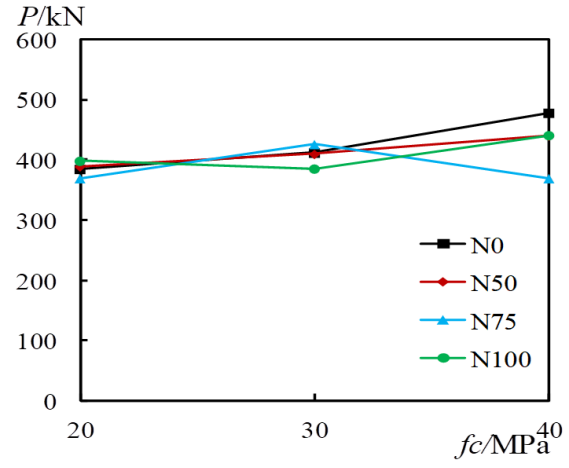

(a) T=1.0mm

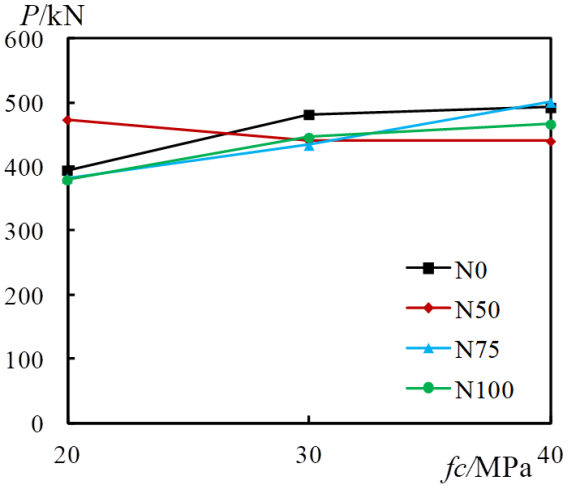

(b) T=1.2mm

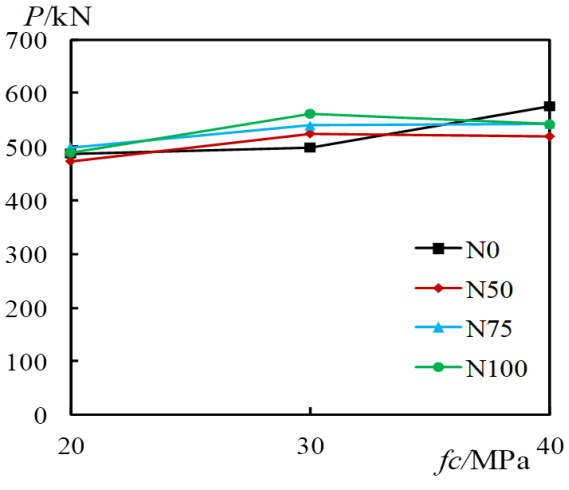

(c) T=1.5mm

Figure 13: P-f_c curves

4.3 Effect of thickness

As seen from Figure 10(f), 10(g), 10(h), and 10(i), the specimens with T=1.5mm have longer elastic stage than that with other wall thickness. The ductility of C-CFSST stub columns with T=1.5mm is the best, and the limit bearing capacity of specimens with T=1.5mm is the largest, which indicates that the specimens with T=1.5mm have the best performance on deformation resistance and load-bearing capacity. It can be explained that the stainless steel tube with high thickness has larger transverse binding force.

Figure 14 shows the influence of wall thickness on the limit bearing capacity of C-CFSST stub columns with same f_c. It could be found that the broken line has an uptrend with the increase of all thickness, which shows that the specimens with greater wall thickness have larger load bearing capacity.

In addition, as seen from Table 5, the limit bearing capacity of some specimens with T=1.5mm subjected to cycle of freeze-thaw is larger than limit bearing capacity of specimens with T=1.5mm without being subjected to cycle of freeze-thaw, which could be explained that the greater wall thickness is, the larger constraining effect to internal nano-silica concrete have, and then the freezing and thawing has strengthened the core concrete of specimens with T=1.5mm.

4.4 Analysis of variables

Figure 15 shows the effect of three parameters on Percentage of force decrease (Per) of specimens subjected to cycle of freeze-thaw. It could be found that the freezing and thawing reduced the bearing capacity. The freezing and thawing has the greatest influence on specimens with f_c=40MPa, and the freezing and thawing has minimal effect on C-CFSST stub columns with f_c=30MPa. However, the specimens with T=1.5mm and f_c=30MPa subjected to cycle of freeze-thaw have larger bearing capacity than the specimens (T=1.5mm and f_c=30MPa) without being subjected to cycle of freeze-thaw, which indicates that freeze-thaw cycles strengthened internal nano-silica concrete of specimens. As seen from Figure 14, the limit bearing capacity of C-CFSST short columns with N=50 has maximum loss, then the loss of l limit bearing capacity of C-CFSST short columns decreased when N to 75, but the loss of limit bearing capacity of specimens became larger when N reached to100.

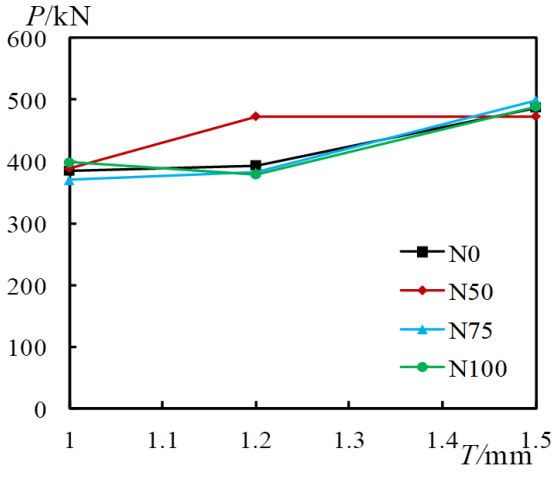

(a) f_c=20MPa

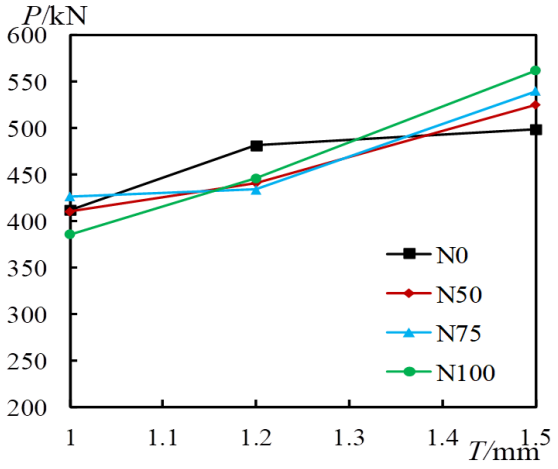

(b) f_c=30MPa

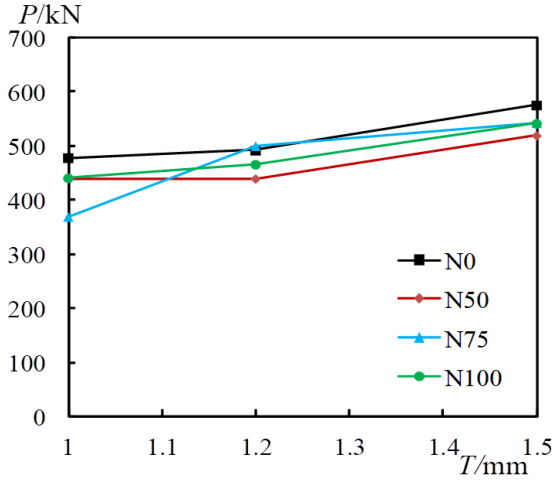

(c) *fc*=40MPa

Figure 14: *P-T* curves

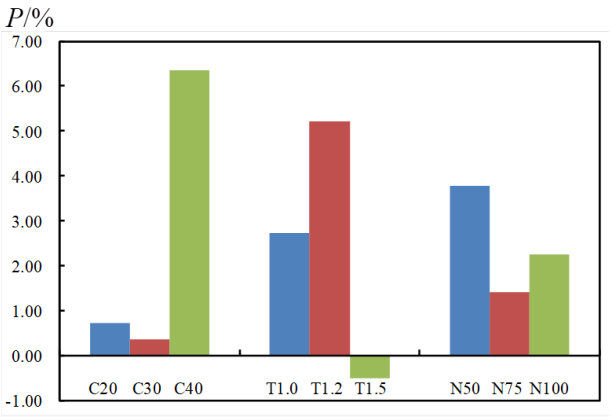

Figure 15: The effect of three parameters on *Per*

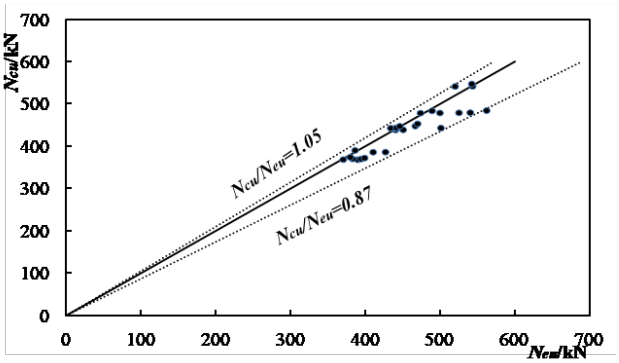

Figure 16: Distribution of N_{cu}/N_{eu}

5 Parameter formulas

It could be found that the limit bearing capacity of specimens is determined by *Kr* (reduction coefficient), which is mainly affected by *T*(wall thickness), f_c(nano-silica concrete strength), *N*(number of freeze-thaw cycles), as shown in the following equation (1).

$$Kr = \frac{N_u}{N_{au}} \tag{1}$$

To simplify the calculation, α and β are introduced, and *Kr* is calculated by equation (2), the definition of f_{c0}, α and β are shown in equation (3).

$$Kr = f(\alpha) \times f(\beta) \times f(N) \tag{2}$$

$$\alpha = \frac{f_c}{f_{c_0}} f_{c_0} = 30\text{MPa and } \beta = \frac{D}{T} \tag{3}$$

D represents the diameter of specimens, *T* represents the wall thickness of specimens, *N* represents the number of freeze-thaw cycles. The functions of α, β and *N* are shown in equation (4), (5), (6).

$$f(\alpha) = -0.063\alpha + 1.045 \tag{4}$$

Table 6: Comparison of calculated ultimate loading capacity between formula and tests

Specimens label	α	β	N	f_{c0}(MPa)	Kr	N_{cu}(kN)	N_{eu}(kN)	N_{cu}/N_{eu}
C20-T1.0-N50	0.67	89.00	50	30	1.01	370.19	389.15	0.95
C30-T1.0-N50	1.00	89.00	50	30	0.99	387.95	409.85	0.95
C40-T1.0-N50	1.33	89.00	50	30	0.92	440.59	439.90	1.00
C20-T1.2-N50	0.67	74.17	50	30	1.00	371.95	393.85	0.94
C30-T1.2-N50	1.00	74.17	50	30	0.92	444.44	440.70	1.01
C40-T1.2-N50	1.33	74.17	50	30	0.89	444.88	439.75	1.01
C20-T1.5-N50	0.67	59.33	50	30	0.97	480.34	473.15	1.02
C30-T1.5-N50	1.00	59.33	50	30	1.05	481.09	524.60	0.92
C40-T1.5-N50	1.33	59.33	50	30	0.90	543.42	519.40	1.05
C20-T1.0-N75	0.67	89.00	75	30	0.96	370.43	369.80	1.00
C30-T1.0-N75	1.00	89.00	75	30	1.03	388.20	426.35	0.91
C40-T1.0-N75	1.33	89.00	75	30	0.94	440.88	449.95	0.98
C20-T1.2-N75	0.67	74.17	75	30	0.97	372.19	382.25	0.97
C30-T1.2-N75	1.00	74.17	75	30	0.90	444.73	433.35	1.03
C40-T1.2-N75	1.33	74.17	75	30	1.02	445.17	500.40	0.89
C20-T1.5-N75	0.67	59.33	75	30	1.02	480.66	499.15	0.96
C30-T1.5-N75	1.00	59.33	75	30	1.08	481.41	539.65	0.89
C40-T1.5-N75	1.33	59.33	75	30	0.94	543.78	542.85	1.00
C20-T1.0-N100	0.67	89.00	100	30	1.04	374.18	398.50	0.94
C30-T1.0-N100	1.00	89.00	100	30	0.94	392.13	385.65	1.02
C40-T1.0-N100	1.33	89.00	100	30	0.92	445.34	441.10	1.01
C20-T1.2-N100	0.67	74.17	100	30	0.96	375.96	379.15	0.99
C30-T1.2-N100	1.00	74.17	100	30	0.93	449.23	445.40	1.01
C40-T1.2-N100	1.33	74.17	100	30	0.95	449.67	466.15	0.96
C20-T1.5-N100	0.67	59.33	100	30	1.00	485.52	488.65	0.99
C30-T1.5-N100	1.00	59.33	100	30	1.13	486.28	561.50	0.87
C40-T1.5-N100	1.33	59.33	100	30	0.94	549.28	541.70	1.01
C40-T1.0-N75 *	1.33	89.00	100	30	0.98	455.07	469.20	0.97
Max								1.05
Min								0.87
Mean								0.97
Vari								0.002

$$f(\beta) = 0.00014\beta^2 - 0.0216\beta + 1.8 \quad (5)$$

$$f(N) = 7.35 \times 10^{-6} \times N^2 - 0.000893 \times N + 0.998 \quad (6)$$

The calculated bearing capacity (N_{cu}) by the formula was compared with the experimental bearing capacity (N_{eu}) of C-CFSST short columns to verify the validity of the formula. As seen from Table 6 and Figure 16, the mean value of N_{cu}/N_{eu} is 0.97, the maximum value is 1.05, the minimum value is 0.87, and the variance is 0.002. The results show that the method has the characteristics of high precision and small fluctuation. Therefore, it is reasonable to use the formula to predict the ultimate bearing capacity of C-CFSST short column under freezing-thawing action. Overall, these forecasts are somewhat conservative.

6 Conclusions

1. The freezing and thawing has little effect on the failure mode of C-CFSST stub columns.
2. On average, the number of freezing and thawing cycles (N) of 50 has maximal influence on limit bearing capacity of specimens, and the influence on limit bearing capacity of specimens decreased when N

reached to 75, finally the influence of N became larger when N reached to 100.

3. The limit bearing capacity of specimens with the same N and nano-silica concrete strength (f_c) increases as the wall thickness (T) increases. The influence of N on the initial stiffness of C-CFSST stub columns decreases with the thickness (T) increases. The specimens with T=1.5mm have the best performance on deformation resistance and maximal load-bearing capacity.
4. The load-bearing capacity of C-CFSST stub columns increases with the increase of f_c of C-CFSST stub columns in limited N. The loss of bearing capacity of f_c=40MPa specimen under freeze-thaw cycle is the biggest, and the loss of bearing capacity of specimens with f_c=30MPa under freeze-thaw cycle is the minimal. The influence of cycle of freeze-thaw on initial stiffness decreases with the nano-silica concrete strength increases.
5. The load-bearing capacity of specimens with f_c=30MPa and T=1.5mm subjected to cycle of freezing and thawing is greater than bearing capacity of specimens with f_c=30MPa and T=1.5mm at normal temperature. It can be explained that the freezing and thawing has strengthened the internal nano-silica concrete of C-CFSST stub columns due to particular mix proportion of C30 and great constraining to nano-silica concrete provided by wall.

Acknowledgement: This research work was supported by the National Natural Science Foundation of China (No. 51778066).

References

[1] Lee J.S., Moving from convergence to divergence: the future of nanotechnology, Nanotechnol. Rev., 2014, 3(5), 411-412.
[2] Khaled R., Brakke E., Sereda G., Fluorescent labeling of materials using silica nanoparticles, Nanotechnol. Rev., 2014, 3(5), 591-596.
[3] Li Z.H., Xu K., Wei F., Recent progress in photodetectors based on low-dimensional nanomaterials, Nanotechnol. Rev., 2018, 7(5), 393-411.
[4] Pawłowski R., Pawłowski B., Wita H., Pluta A., Sobik P., Sala A., Łanuszewska A., Patsula V., Drabczyk K., Jakubowska M., Silver nanoparticles in the thermal silver plating of aluminium busbar joints, Nanotechnol. Rev., 2018, 7(5), 365-372.
[5] Robinson C.A.J., Rajesh S., Current trends in changing the channel in MOSFETs by III-V semiconducting nanostructures, Nanotechnol. Rev., 2017, 6(6), 613-623.
[6] Zhang H.L., Selective modification of inner surface of halloysite nanotubes: a review, Nanotechnol. Rev., 2017, 6(6), 573-581.
[7] Gupta M., Kumar M., Effect of nano silica and coir fiber on compressive strength and abrasion resistance of concrete, Constr. Build. Mater., 2019, 226, 44-50.
[8] Alhawat M., Ashour A., Bond strength between corroded steel and recycled aggregate concrete incorporating nano silica, Constr. Build. Mater., 2020, 237, 117441.
[9] Svintsov A.P., Shchesnyak E.L., Galishnikova V.V., Fediuk R.S., Stashevskaya N.A., Effect of nano-modified additives on properties of concrete mixtures during winter season, Constr. Build. Mater., 2020, 237, 117527.
[10] Hassanein M.F., Kharoob O.F., Analysis of circular concrete-filled double skin tubular slender columns with external stainless steel tubes, Thin. Wall. Struct., 2014, 79, 23-37.
[11] Patel V.I., Liang Q.Q., Hadi M.N.S., Nonlinear analysis of circular high strength concrete-filled stainless steel tubular slender beam-columns, Eng. Struct., 2017, 130, 1-13.
[12] Han L.H., Ren Q.X., Li W., Tests on stub stainless steel-concrete-carbon steel double-skin tubular (DST) columns, J. Constr. Steel. Res., 2011, 67(3), 437-452.
[13] Uy B., Tao Z., Han L.H., Behaviour of short and slender concrete-filled stainless steel tubular columns, J. Constr. Steel. Res., 2011, 67(3), 360-378.
[14] Zhao O., Gardner L., Young B., Structural performance of stainless steel circular hollow sections under combined axial load and bending-Part2: Parametric studies and design, Thin. Wall. Struct., 2016, 101, 240-248.
[15] Yuan H.X., Wang Y.Q., Shi Y.J., Gardner L. Residual stress distributions in welded stainless steel sections, Thin. Wall. Struct., 2014, 79, 38-51.
[16] Jandera M., Machacek J., Residual stress influence on material properties and column behavior of stainless steel SHS, Thin. Wall. Struct., 2014, 83, 12-18.
[17] Yang Y.F., Cao K., Wang T.Z., Experimental behavior of CFST stub columns after being exposed to freezing and thawing, Cold Reg. Sci. Technol., 2013, 89, 7-21.
[18] Li B., Mao J., Nawa T., Liu Z., Mesoscopic chloride ion diffusion model of marine concrete subjected to freeze-thaw cycles, Constr. Build. Mater., 2016, 125, 337-351.
[19] Penttala V., Al-Neshawy F., Stress and strain state of concrete during freezing and thawing cycles, Cem. Concr. Res., 2002, 32(9), 1407-1420.
[20] Tian J., Wang W., Du Y., Damage behaviors of self-compacting concrete and prediction model under coupling effect of salt freeze-thaw and flexural load, Constr. Build. Mater., 2016, 119, 241-250.
[21] Shang H.S., Wang Z.H., Zhang P., Zhao T.J., Fan G.X., Ren G.S., Bond behavior of steel bar in air-entrained RCAC in fresh water and sea water after fast freeze-thaw cycles, Cold Reg. Sci. Technol., 2017, 135, 90-96.
[22] Haddad R.H., Numayr K.S., Effect of alkali-silica reaction and freezing and thawing action on concrete-steel bond, Constr. Build. Mater., 2007, 21(2), 428-435.
[23] Shang H.S., Song Y.P., Experimental study of strength and deformation of plain concrete under biaxial compression after freezing and thawing cycles, Cem. Concr. Res., 2006, 36(10), 1857-1864.
[24] Gonzalez M., Tighe S., Hui K., Rahman S., De Oliveira Lima A., Evaluation of freeze/thaw and scaling response of nanoconcrete for portland cement concrete (PCC) pavements, Constr. Build. Mater., 2016, 120, 465-472.
[25] Their J.M., Özakça M., Developing geopolymer concrete by using cold-bonded fly ash aggregate, nano-silica, and steel fiber,

Constr. Build. Mater., 2018, 180, 12-22
[26] Li L.G., Zheng J.Y., Ng P.L., Zhu J., Kwan A.K.H., Cementing efficiencies and synergistic roles of silica fume and nano-silica in sulphate and chloride resistance of concrete, Constr. Build. Mater., 2019, 223, 965-975.
[27] Shafiq N., Kumar R., Zahid M., Tufail R.F., Effects of modified metakaolin using nano-silica on the mechanical properties and durability of concrete, Materials (Basel, Switzerland), 2019, 12(14), 2291.
[28] Zhang T., Lyu X.T, Yu Y., Prediction and analysis of the residual capacity of concrete-filled steel tube stub columns under axial compression subjected to combined freeze–thaw cycles and acid rain corrosion, Materials (Basel, Switzerland), 2019, 12(19), 3070.
[29] Chinese Code, Metallic materials-tensile testing at ambient temperature, GB/T 228-2002, BeiJing China, 2002(in Chinese).
[30] GB/T. 50082-2009, 2009., Standard for test methods of long-term performance and durability of ordinary concrete, China Architecture & Building Press, Beijing (in Chinese).